Magnetization-induced optical third-harmonic generation in Co and Fe nanostructures

O.A. Aktsipetrov,* E.M. Kim, R.V. Kapra, and T.V. Murzina†
Department of Physics, Moscow State University, 119992 Moscow, Russia

A.F. Kravets
Institute of Magnetism, National Academy of Sciences of Ukraine, Kiev, 03680 Ukraine

M. Inoue
Toyohashi University of Technology, Toyohashi 441-8580 Japan

S.V. Kuznetsova, M.V. Ivanchenko, and V.G. Lifshits
Institute of Automation and Control Processes, 690041 Vladivostok, Russia
(Dated: February 2, 2008)

Magnetization-induced optical third-harmonic generation (MTHG) is observed in magnetic nanostructures: Co and Fe nanolayers and granular films containing Co nanoparticles. Magnetization-induced variations of the MTHG characteristics in these nanostructures exceed the typical values of linear magneto-optical Kerr effect by at least an order of magnitude: the maximum of magnetic contrast in the MTHG intensity is up to 0.2, the angle of polarization rotation for MTHG is 10° and the relative phase shift is up to 100°.

PACS numbers:

Magneto-optics, with its more than century-long history, remains one of the most important experimental methods in studies of magnetism. Recently, significant attention has been directed towards nonlinear magneto-optics [1]: nonlinear magneto-optical Faraday and Kerr effects in second-harmonic generation (SHG) were observed experimentally in yttrium-iron-garnet films [2], then at surfaces of magnetic metals [3], in magnetic multilayers [4] and nanogranules [5]. Experimental measurements [2-5] and theoretical estimates [6] reveal the typical magnitudes of the magnetization-induced effects in SHG: the magnetization-induced variations of the SHG intensity and rotation of the second-harmonic (SH) wave polarization, may exceed the linear magneto-optical Kerr effect (MOKE) by orders of magnitude.

It is well recognized that magnetization-induced SHG (MSHG) is a powerful probe of surface and interface magnetism [1,6,7]. The latter comes about from the lack of dipole magnetization-induced second-order susceptibility in the bulk of centrosymmetric magnetic materials. In contrast to the bulk, the surface of centrosymmetric materials is always noncentrosymmetric and results in localization of the dipole magnetization-induced nonlinear polarization at the surface. MSHG comes from the surface layer that is several nanometers thick and probes the surface magnetic properties. Meanwhile, this high surface sensitivity of MSHG is extruded in shadow third-order nonlinear magneto-optical effects because of their bulk localization as well as their small expected value. This is why the observation of magnetization-induced third-harmonic generation (MTHG) is discussed just recently in garnet films [8,9] and magnetic alloys [10]. On the other hand, both the surface MSHG and bulk MTHG are expected to supplement each other as magneto-optical probes and provide complementary information about the magnetic properties of nanostructures.

In this paper, magnetization-induced THG is observed in the following magnetic nanostructures: Co and Fe nanolayers, and granular films containing Co nanoparticles.

For the description of MTHG, one can follow the phenomenological approach which has been developed for the MSHG effects [1]. According to this approach, the third-order susceptibility of a magnetic material is a combination of crystallographic and magnetic terms, which possess *even* and *odd* parities in magnetization, M, respectively: $\chi^{(3)}_{ijkl} = \chi^{(3)cryst}_{ijkl} + \chi^{(3)odd}_{ijkl}(M)$, where $\chi^{(3)cryst}_{ijkl}(M)=\chi^{(3)cryst}_{ijkl}(-M)$ is the crystallographic nonmagnetic susceptibility and $\chi^{(3)odd}_{ijkl}(M)=-\chi^{(3)odd}_{ijkl}(-M)$ is the magnetic susceptibility. Then the MTHG intensity is given by:

$$I_{3\omega}(M) \sim [\mathbf{E}^{cryst}_{3\omega} + \mathbf{E}^{odd}_{3\omega}(M)]^2 = [f_i(3\omega)(\chi^{(3)cryst}_{ijkl} + \chi^{(3)odd}_{ijkl}(M))f_j(\omega)f_k(\omega)f_l(\omega)E_j(\omega)E_k(\omega)E_l(\omega) + c.c.]^2, \quad (1)$$

where $E_i(\omega)$ is the i-th component of the fundamental field, $\mathbf{E}^{cryst}_{3\omega}$ and $\mathbf{E}^{odd}_{3\omega}(M)$ are the third-harmonic (TH) fields originating from the crystallographic and magnetic susceptibilities, respectively, $f_i(3\omega)$ and $f_j(\omega)$ are coefficients that contain Fresnel and local field factors and linear magneto-optical rotation of polarization of fields at corresponding wavelengths. Eq. 1 includes a cross-product of $\mathbf{E}^{cryst}_{3\omega}$ and $\mathbf{E}^{odd}_{3\omega}(M)$. This interference cross-product, $\mathbf{E}^{odd}_{3\omega}(M) \cdot \mathbf{E}^{cryst}_{3\omega}$, is *odd* with respect to mag-

*Electronic address: aktsip@shg.ru
†Electronic address: mur@shg.ru

netization and is responsible for the internal homodyne effect [11]. The absolute value of homodyne cross-term is not supposed to be small, even for an intrinsically small magnetic co-factor, because of the large value of crystallographic co-factor. To describe the intensity effects in MTHG, the THG magnetic contrast, $\rho_{3\omega}$, can be defined by analogy with the SHG magnetic contrast, $\rho_{2\omega}$, introduced in [3,4]:

$$\rho_{3\omega} = \frac{I_{3\omega}(M\uparrow) - I_{3\omega}(M\downarrow)}{I_{3\omega}(M\uparrow) + I_{3\omega}(M\downarrow)} \sim \frac{\chi_{eff}^{(3)odd}(M)}{\chi_{eff}^{(3)cryst}} \cos[\Phi_{3\omega}(M)], \tag{2}$$

where $I_{3\omega}(M\uparrow\downarrow)$ are the THG intensities for the opposite directions of the magnetization, $\chi_{eff}^{(3)odd}(M)$ and $\chi_{eff}^{(3)cryst}$ are the combinations of tensor components of the corresponding susceptibilities and $\Phi_{3\omega}(M)$ is the relative phase between $\mathbf{E}_{3\omega}^{cryst}$ and $\mathbf{E}_{3\omega}^{odd}(M)$. Symmetry analysis of $\chi_{ijkl}^{(3)odd}(M)$ tensor [8,9] shows that magnetization-induced variations of the THG intensity result from the internal homodyne effect in the geometry of the transversal Kerr effect (see the left-hand inset in Figure 1, *a*). To extract the ratio of *magnetic* and *crystallographic* components of $\chi_{eff}^{(3)}$ from $\rho_{3\omega}$, one should obtain $\Phi_{3\omega}(M)$ from the THG interferometry.

The THG interferometry is the direct analogue of the SHG interferometry described in detail elsewhere [12]. The scheme of the nonlinear optical interferometry is shown at the right-hand inset in Fig. 1 a). The TH fields from the sample and the reference source interfere at the photomultiplier while the reference THG source is translated along the direction of the fundamental beam. The interference pattern, i.e., an oscillating dependence of the detected THG intensity as a function of the reference displacement, r, results from the phase shift between the interfering TH fields. This shift appears in the space between the sample and the reference due to the dispersion of air at the TH and fundamental wavelengths. The total THG intensity from a magnetic sample and a nonmagnetic reference as a function of r is given by:

$$I_{3\omega}(r,M) = I_{3\omega}^{ref} + I_{3\omega}^{samp}(M) + 2\alpha\sqrt{I_{3\omega}^{ref} I_{3\omega}^{samp}(M)} \cos[\frac{2\pi r}{L(3\omega)} + \Phi_{3\omega}^{samp}(M) - \Phi_{3\omega}^{ref}], \tag{3}$$

where $L(3\omega) = \lambda_\omega(3\Delta n)^{-1}$ is the interference pattern period, λ_ω is the fundamental wavelength, α is the coherence coefficient of the fundamental beam, $\Delta n = n(3\omega) - n(\omega)$ describes the dispersion of the refractive index of air, n, at the THG and fundamental wavelengths, respectively, $\Phi_{3\omega}^{samp}(M) \equiv arg[E_{3\omega}^{samp}(M)]$ and $\Phi_{3\omega}^{ref} \equiv arg[E_{3\omega}^{ref}]$ are the phases of the TH fields from the magnetic sample, $\mathbf{E}_{3\omega}^{samp}(M)$, and the reference THG source, $\mathbf{E}_{3\omega}^{ref}$, respectively. The magnetization-induced shift between two interference patterns measured for the opposite directions of the magnetic field, $\varphi_{3\omega}(M) = \Phi_{3\omega}^{samp}(M\uparrow) - \Phi_{3\omega}^{samp}(M\downarrow)$, allows one to deduce $\Phi_{3\omega}(M)$ in accordance with the vector diagram at the inset in Fig. 1, b).

The samples of magnetic nanostructures studied in this work are: (1) magnetic nanogranular films of the composition Co_xAg_{1-x} and $Co_x(Al_2O_3)_{1-x}$ and (2) thin homogeneous Co and $Fe(110)$ films. The Co_xAg_{1-x} and $Co_x(Al_2O_3)_{1-x}$ films are prepared by the co-evaporation of Co and Ag (Al_2O_3) from two independent electron-beam sources onto glass-ceramic substrates [13]. The structure of Co_xAg_{1-x} and $Co_x(Al_2O_3)_{1-x}$ films is characterized by X-ray diffraction and reveals the existence of nanogranules with the diameter ranging from 3 nm to 6 nm for the composition $x < 0.4$. The fabricated granular films exhibit giant magnetoresistance (GMR) effects that are characterized by the GMR coefficient: $\rho_{GMR} = -[R(0) - R(M)]/R(0)$, where $R(M)$ and $R(0)$ is Ohmic resistance measured in magnetized and demagnetized material. ρ_{GMR} is measured by the four-probe method at room temperature in a magnetic field up to 8 kOe.

Homogeneous Co films 400 nm thick are deposited in similar conditions using a single Co source. The homogeneous $Fe(110)$ films 100 nm thick are epitaxially grown on $Si(111)$ substrates [14].

The output of an OPO laser system "Spectra-Physics 710" at 800 nm wavelength, pulse duration of 4 ns, pulse intensity of 2 MW/cm^2, and a Q-switched $YAG:Nd^{3+}$ laser at 1064 nm wavelength, pulse duration of 15 ns and pulse intensity of 1 MW/cm^2 are used as the fundamental radiation. The TH(SH) radiation is filtered out by appropriate glass bandpass and interference filters and is detected by a PMT and gated electronics. To normalize the THG(SHG) signal over the OPO and $YAG:Nd^{3+}$ laser fluency and the spectral sensitivity of the optical detection system, a reference channel is used with a Z-cut quartz plate as a reference and a detection system identical to that in the "sample" channel. The THG and SHG interferometry is performed by translating a 30 nm thick indium-tin-oxide (ITO) film on a glass substrate in the direction parallel to the laser beam. An in-plane dc-magnetic field up to 2 kOe is applied in nonlinear magneto-optical measurements at the magnetic samples by permanent Fe-Nd magnets.

Prior to the studies of magnetization-induced effects in THG, Co and Fe nanostructures are characterized by the MSHG probe. Table 1, column 2, presents the SHG magnetic contrast for all samples. The largest value of $\rho_{2\omega}$ is up to 0.45 in $Fe(110)$ homogeneous nanolayers.

The experimental values of $\rho_{3\omega}$ in Co and Fe nanostructures are presented in the Table 1, column 1. In particular, $\rho_{3\omega}$ in $Co_{0.19}(Al_2O_3)_{0.81}$ is up to 0.16, which exceeds the linear MOKE by about two orders of magnitude [15]. The comparison of $\rho_{3\omega}$ and $\rho_{2\omega}$ in the same materials shows that for nanogranular films the magnetic contrast in THG and SHG is nearly the same, while in Co and Fe nanolayers $\rho_{2\omega}$ is several times larger than $\rho_{3\omega}$.

Figure 1 shows two THG interference patterns for Co

	$\rho_{3\omega}$	$\rho_{2\omega}$	$\varphi_{3\omega}(M)$	$\varphi_{2\omega}(M)$	$\chi_{eff}^{(3)odd}(M)/\chi_{eff}^{(3)cryst}$	$\chi_{eff}^{(2)odd}(M)/\chi_{eff}^{(2)cryst}$
Co	0.09 ± 0.03	0.32 ± 0.05	$70^0 \pm 10^0$	$14^0 \pm 4^0$	0.55 ± 0.1	0.2 ± 0.05
$Fe(110)$	0.08 ± 0.03	0.45 ± 0.05	$9^0 \pm 5^0$	$13^0 \pm 4^0$	0.09 ± 0.05	0.3 ± 0.05
$Co_{0.31}Ag_{0.69}$	0.09 ± 0.03	0.05 ± 0.03	$17^0 \pm 5^0$	$8^0 \pm 3^0$	0.16 ± 0.05	0.1 ± 0.05
$Co_{0.19}(Al_2O_3)_{0.81}$	0.16 ± 0.04	0.09 ± 0.03	$105^0 \pm 15^0$	$14^0 \pm 5^0$	1.3 ± 0.1	0.13 ± 0.05

TABLE I: Magnetic contrast in the THG and SHG intensity; the magnetization-induced phase shift of the total TH, $\varphi_{3\omega}(M)$, and SH, $\varphi_{2\omega}(M)$, fields; the ratio of $\chi_{eff}^{(3)odd}(M)/\chi_{eff}^{(3)cryst}$ and $\chi_{eff}^{(2)odd}(M)/\chi_{eff}^{(2)cryst}$ for magnetic nanostructures.

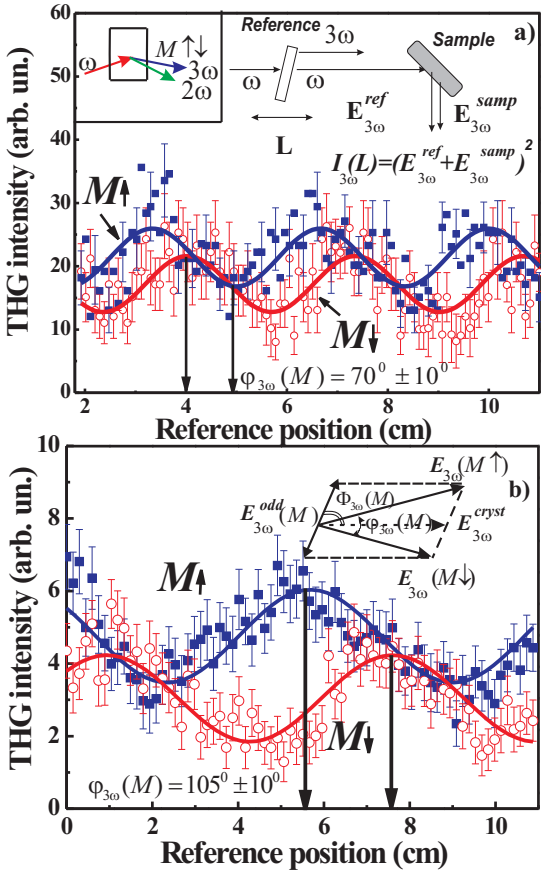

FIG. 1: (a) The MTHG interferometry patterns in Co film for the opposite directions of the magnetization, $M \uparrow\downarrow$. Left-hand inset: the scheme of the transversal geometry of nonlinear magneto-optical Kerr effect. Right-hand inset: the scheme of SHG and THG interferometry. (b) The MTHG interferometry patterns in $Co_{0.19}(Al_2O_3)_{0.81}$ film for the opposite directions of the magnetization $M \uparrow\downarrow$. Inset: vector diagram of odd and crystallographic components of the TH field.

and $Co_{0.19}(Al_2O_3)_{0.81}$ films for the opposite directions of magnetization and the magnetization-induced phase shift for $\varphi_{3\omega}(M) = 70^0$ and 105^0, respectively, is observed for the total TH field, $\mathbf{E}_{3\omega}(M)$. Results of interferometric measurements of the relative phase shift of magnetization-induced TH field and the ratio of the magnetic and crystallographic components of the third-order susceptibility are summarized in Table 1. Also shown are the results of the analogous MSHG measurements which are presented for comparison with second- and third-order nonlinear magneto-optical effects.

In the longitudinal NOMOKE configuration, the nonmagnetic and magnetization-induced components of the TH field are polarized orthogonally, $\mathbf{E}_{3\omega}^{cryst}$ being p-polarized and $\mathbf{E}_{3\omega}^{odd}(M)$ being s-polarized, respectively. The magnetization-induced effects appear in the rotation of polarization of the total TH wave. The THG intensity depends on the analyzer angle Θ:

$$I_{3\omega}(\Theta) \propto |\mathbf{E}_{3\omega}^{cryst} \cos\Theta + \mathbf{E}_{3\omega}^{odd}(M) \exp(i\phi_M) \sin\Theta|^2, \quad (4)$$

where the phase shift ϕ_M describes the TH field ellipticity. The TH wave is considered to be linearly polarized with $\phi_M \simeq 0$. The rotation angle of the polarization of the TH wave upon reversal of magnetization is estimated to be $\Delta\Theta \simeq 2\arctan[|\mathbf{E}_{3\omega}^{odd}(M)|/|\mathbf{E}_{3\omega}^{cryst}|]$ and depends on the ratio of corresponding elements of the $\chi_{ijkl}^{(3)odd}(M)$ and $\chi_{ijkl}^{(3)cryst}$ tensors [10]. Magnetization-induced rotation of the TH wave polarization up to $10^0 \pm 2^0$ is observed in $Fe(110)$ nanolayers. The previously mentioned magnetization-induced effects in THG are attributed to the proper combinations of components of magnetic and crystallographic third-order susceptibilities. In principle, the part of magnetization-induced changes in the THG parameters might originate from linear MOKE at the fundamental wavelength. Meanwhile, magnetization-induced changes of the amplitude and polarization of the fundamental wave show that corresponding contributions to MTHG are negligible.

The observation of magnetization-induced effects in THG from Co_xAg_{1-x} and $Co_x(Al_2O_3)_{1-x}$ nanogranular films allows one to perform a comparative analysis of MTHG and GMR effects as it was performed recently for MSHG in Co_xAg_{1-x} films [5]. Figure 2, *a* shows the dependence of $\rho_{3\omega}$ on the concentration of Co in Co_xAg_{1-x} films, which reveals a monotonic increase for $x > 0.4$ and a local maximum in the vicinity of $x \approx 0.3$. The former corresponds to a straightforward monotonic increase of the ferromagnetic phase in the Co fraction of the composite material as the concentration of Co exceeds the percolation threshold [10]. A local maximum corresponds to the specific magnetic properties of nanogranules; $\rho_{3\omega}(x)$

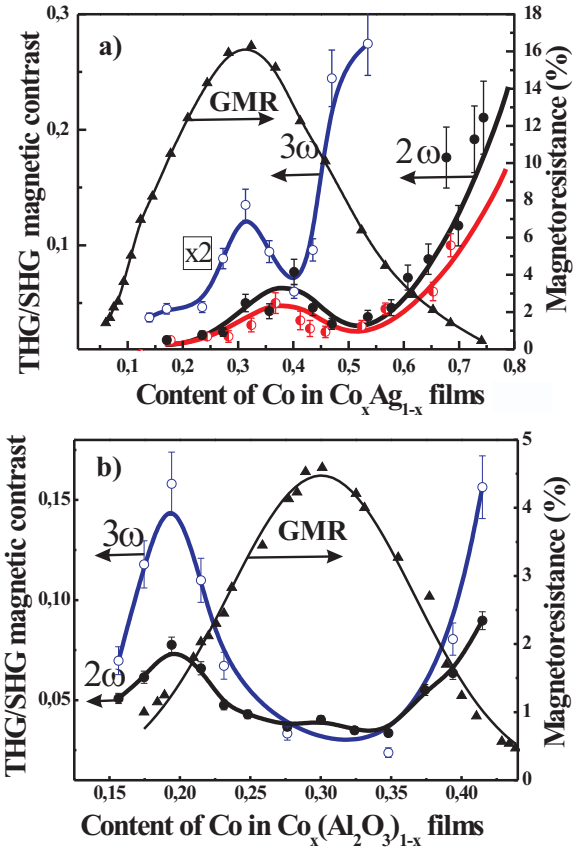

FIG. 2: (*a*) Magnetic contrast in the THG intensity for Co_xAg_{1-x} nanogranular films as a function of the film composition x (shown with open circles). The SHG magnetic contrast at the fundamental wavelength of 1064nm (closed circles), and 800nm (half-closed circles), respectively. Magnetoresistance as a function of the Co_xAg_{1-x} film composition x (triangles). (*b*) Magnetic contrast in the THG intensity for $Co_x(Al_2O_3)_{1-x}$ nanogranular films as a function of the film composition x (open circles). Magnetic contrast in the SHG intensity (closed circles). The GMR coefficient as a function of the $Co_x(Al_2O_3)_{1-x}$ film composition x (triangles).

attains a local maximum at the same region of Co concentration (0.3 - 0.35) as the concentration dependence of ρ_{GMR}. It is worth noting that correlation between $\rho_{3\omega}(x)$ and $\rho_{GMR}(x)$ is almost the same as for $\rho_{2\omega}(x)$ as presented in Figure 2, *a* for comparison. The maximum of $\rho_{2\omega}(x)$, measured at two wavelengths of the fundamental radiation of 800 nm and 1064 nm, is attained in the vicinity of $x \approx 0.36$. The similarity of the dependencies of $\rho_{2\omega}$ and ρ_{GMR} on x in Co_xAg_{1-x} nanogranular films has recently [5] been supposed to originate from the dependence of the nonlinear optical response and the GMR effect on the quality of interfaces between magnetic granules and the nonmagnetic host material. In fact, GMR in Co_xAg_{1-x} nanogranular films is attributed to the spin-dependent electron *scattering* and is highly interface sensitive [13].

The connection between the GMR mechanism and the correlation between $\rho_{3\omega/2\omega}(x)$ and $\rho_{GMR}(x)$ becomes more apparent from the comparison of the MTHG and MSHG results in two different types of nanogranular films. In contrast to spin-dependent electron *scattering* in Co_xAg_{1-x} films, the GMR effect in $Co_x(Al_2O_3)_{1-x}$ films is attributed to spin-dependent electron *tunnelling* [16]. Figure 2, *b* shows the dependencies of $\rho_{3\omega/2\omega}$ on the concentration of Co in $Co_x(Al_2O_3)_{1-x}$ films. Qualitatively, these dependencies are close to those in Co_xAg_{1-x} films. Meanwhile, contrary to Co_xAg_{1-x} films, the local maximum of both $\rho_{3\omega}(x)$ and $\rho_{2\omega}(x)$ is attained at approximately $x \approx 0.19$, whereas the peak of $\rho_{GMR}(x)$ is centered at $x \approx 0.3$. This shift between maxima of $\rho_{3\omega/2\omega}(x)$ and $\rho_{GMR}(x)$ in $Co_x(Al_2O_3)_{1-x}$ films shows the lack of correlation between nonlinear magneto-optical and GMR effects in this material.

In conclusion, magnetization-induced optical third-harmonic generation is observed in magnetic homogeneous Fe and Co nanolayers and magnetic films containing Co nanogranules. Magnetization-induced variations of the THG parameters are of the same order of magnitude as in MSHG, and exceed the typical values of the linear MOKE by at least an order of magnitude. Correlation between the dependencies of $\rho_{3\omega/2\omega}(x)$ and $\rho_{GMR}(x)$ is observed below the percolation threshold in Co_xAg_{1-x} films, which reveals the spin-dependent *scattering* GMR mechanism, whereas in $Co_x(Al_2O_3)_{1-x}$ films with the spin-dependent *tunnelling* GMR mechanism, the dependencies of $\rho_{3\omega/2\omega}(x)$ and $\rho_{GMR}(x)$ do not correlate. At the same time, the general conclusion about correlation between MTHG and GMR in Co_xAg_{1-x} films demands further detailed studies.

Acknowledgments

This work is supported in part by the International Association (INTAS) Grant No. 03-51-3784, the Grant-In-Aid from the Ministry of Education, Science, Culture and Sport of Japan No. 14655119 and the Presidential Grant for Leading Russian Science Schools No. 1604.2003.2.

[1] Ru-Pin Pan, H.D. Wei, Y.R. Shen, Phys.Rev.B, **39**, 1229(1989).

[2] O.A. Aktsipetrov, O.V. Braginskii, and D.A. Esikov, Sov. J. Quantum Electron. **20**, 259 (1990).

[3] J. Reif, J.C. Zink, C.-M. Schneider, and J. Kirschner, Phys. Rev. Lett. **67**, 2878(1991).
[4] B. Koopmans, M.G. Koerkamp, Th. Rasing, and H. van den Berg, Phys. Rev. Lett. **74**, 3692 (1995).
[5] T.V. Murzina, et al., Surf. Sci. **482-485**, 1101 (2001).
[6] W. Hübner and K. H. Bennemann, Phys. Rev. B **52**, 13411 (1995).
[7] Th. Rasing, J. Magn. Soc. Jpn. **20**, 13 (1996).
[8] T.V. Murzina, et al., JETP Lett. **77**, 537 (2003)].
[9] J. Shimura, S. Ohkoshi and K. Hashimoto, Appl. Phys. Lett. **82**, 3290 (2003).
[10] T.V. Murzina, et al., JETP Lett. **79**, 155 (2004).
[11] G. Berkovic, Y.R. Shen, G. Marowsky, and R. Steinhoff, J. Opt. Soc. Am. B **6**, 205 (1989).
[12] R. Stolle, G. Marowsky, E. Schwarzberg, G. Berkovic, Appl. Phys. B **63** 491 (1996).
[13] Yu.G. Pogorelov, et al., Phys. Rev. B **60**, 12200 (1999).
[14] L.A. Chebotkevich, et al., Phys. Low-Dim. Struct. **9/10** 141 (2003).
[15] O.A. Aktsipetrov, et al., J. Magn. Magn. Mater. **80**, 196 (1999).
[16] M.N. Baibich, et.al., Phys. Rev. Lett. **61**, 2472 (1988).